CHALMERS
UNIVERSITY OF TECHNOLOGY

A Broad-Band Dual-Polarization All-Metal Dichroic Filter for Cryogenic Applications in Sub-THz Range

Citation for the original published paper (version of record):
Montofre, D., Meledin, D., López, C. et al (2024). A Broad-Band Dual-Polarization All-Metal Dichroic Filter for Cryogenic Applications in Sub-THz
Range. IEEE Transactions on Terahertz Science and Technology, 14(2).
http://dx.doi.org/10.1109/TTHZ.2023.3338472

(article starts on next page)

T-TST-REG-07-2023-00122.R1

A Broad-Band Dual-Polarization All-Metal Dichroic Filter for Cryogenic Applications in Sub-THz Range

Daniel Montofré, Denis Meledin, Cristian Daniel Lopéz, Igor Lapkin, Vincent Desmaris, Leif Helldner, Mathias Fredrixon, Sven-Erik Ferm, and Victor Belitsky, *Senior Member, IEEE*

***Abstract*—In this work, we report on the design and characterization of an all-metal, wideband single-layer dichroic filter operating at non-normal beam incidence. The dichroic filter consists of a perforated metal plate with an angular offset of the perforated channels equal to the beam incidence angle onto the dichroic surface. The fabricated filter is characterized using an especially designed quasi-optical test system. The filter demonstrates 96% transmission of the incoming electromagnetic radiation averaged in the signal band about 37-50 GHz for both polarizations while simultaneously achieving a rejection better than 20 dB for frequencies lower than 26 GHz at the designed beam incidence of 13 degrees. The cross-polarization level for each polarization is better than 30 dB in the passband. The experimental results of the transmission measurements are in very good agreement with electromagnetic simulations confirming the feasibility and benefits of our proposed design concept even at THz frequencies. The simulations of the dichroic scaled version demonstrate that, for instance, it can be employed in the Event Horizon Telescope project, where the 230 GHz and the 345 GHz receiver channels could be operating simultaneously.**

***Index Terms*—Dichroic, Event Horizon Telescope, frequency selective surface, millimeter/submillimeter wave, radio astronomy instrumentation, THz, transmission, VLBI.**

I. INTRODUCTION

MULTI-BAND receiving systems have gained significant popularity as a solution for instrumentation in environmental sciences and radio astronomy [1]. In such systems, the receiver channels run simultaneously while the receivers' spatial pointing is aligned. The use of broadband frequency receivers offers several advantages. In continuum observations, increasing the instantaneous bandwidth directly enhances the power of the received signal. For spectral line observations, a wider instantaneous frequency band enables quicker spectral line surveys or simultaneous observations of astronomically important CO lines, such as J = 2→1 and J = 3→2 transitions at 230 GHz and 345 GHz [2]. Moreover, multi-frequency receiver systems allow simultaneous calibration of the different receiver bands, leading to an improved cross-correlation of the measured lines' intensities compared to individual observations of the same spectral lines. Additionally, such multi-frequency systems can utilize the lower frequency band to calibrate with better accuracy, removing atmospheric noise contributions and introducing phase corrections for higher frequency bands in interferometric observations, as exemplified by the Atacama Large Millimeter Array (ALMA) [3], and millimeter wavelength Very Large Baseline Interferometry (mm-VLBI) [4], which includes Event Horizon Telescope (EHT) [5]. For instance, the ALMA Band 3 channel observing a water maser at a frequency around 86 GHz is used to measure and calibrate out the atmospheric phase contribution for each antenna of the interferometer, while the actual observations occur using the higher frequency channels. In the receiver described in [4], all separate frequency channels are co-aligned on the sky, enabling an accurate accounting of atmospheric noise and phase contributions, thereby significantly improving the observation quality.

One possible implementation of a multi-band receiver system relies on duplexing and filtering techniques using waveguide technology, as presented in [2]. However, the inclusion of diplexers and filters between the feed and the receivers, along with the associated signal (RF) transmission loss, inevitably contributes to an increased system noise. Moreover, these systems often have limitations on the frequency coverage of the available receiver bands due to the constraints of waveguide single-mode operation.

In cases where different receiver channels cannot share the same waveguide due to significant differences in operating frequencies, optical frequency-selective components could be employed, particularly dichroic filters. These components specifically suited for mm and THz frequencies [6], have gained significant attention recently, as they are frequency selective and have low transmission loss. The dichroic filters integrated as part of tertiary optics enable the combination of at most two receiver channels by reflecting the lower frequency

Date of submission: July 14, 2023. *(Corresponding author: Denis Meledin).*

Daniel Montofré was with Group for Advanced Receiver Development (GARD), Department of Space, Earth and Environment, Chalmers University of Technology, 41296 Gothenburg, Sweden, now he is with WoodTech S.A., 7550107, Santiago, Chile (e-mail: montofre@chalmers.se).

Denis Meledin, Cristian Daniel Lopéz, Igor Lapkin, Vincent Desmaris, Leif Helldner, Mathias Fredrixon, Sven-Erik Ferm, Victor Belitsky are with the Group for Advanced Receiver Development (GARD), Department of Space, Earth and Environment, Chalmers University of Technology, 41296 Gothenburg, Sweden.(e-mail: denis.meledin@chalmers.se, cristian.lopez@chalmers.se, igor.lapkin@chalmers.se, vincent.desmaris@chalmers.se, leif.helldner@chalmers.se, mathias.fredrixon@chalmers.se, sven-erik.ferm@chalmers.se, victor.belitsky@chalmers.se).

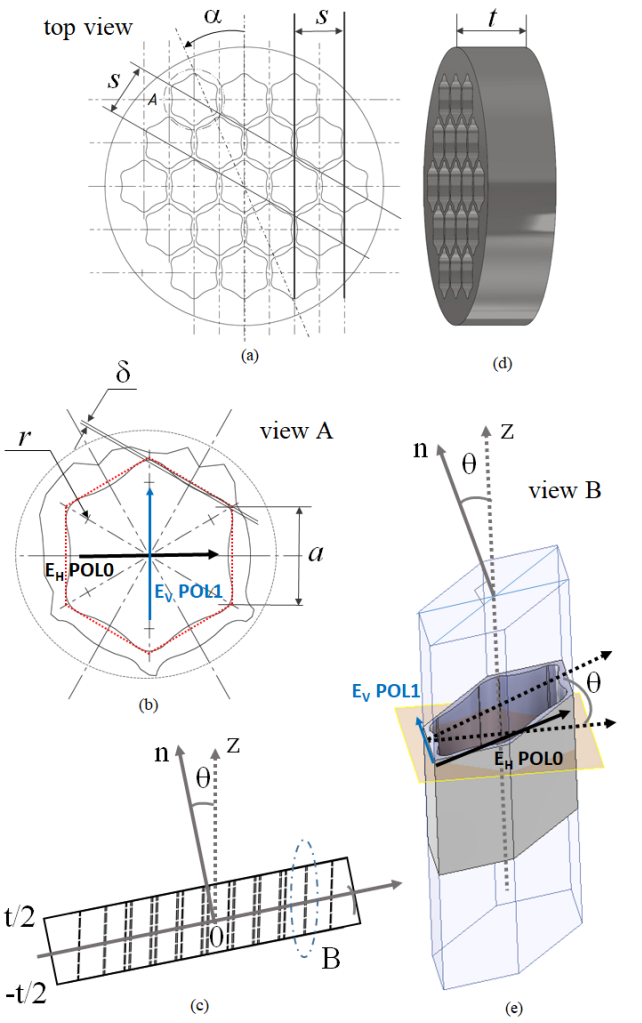

Fig. 1. The geometry of the designed perforated plate: (a) top view from *n* direction; (b) detailed top view A of the dichroic aperture from *n* direction, the hexagon's corners and shape are modified with radius *r* and parameter δ; (c) and (d) - side view of the dichroic plate; (e) - detailed side view B of the single dichroic aperture. The incident wave illuminates the dichroic plate with the angular offset of the apertures θ from the direction of $z=\infty$. Parameter *a* is a side length of the initial hexagonal aperture marked with a red color dot line. The top view is taken from the n-direction. The splitting plane is normal to the axis of the waveguide aperture wall.

band while transmitting the higher frequency band, therefore acting as a high-pass filter. A comprehensive review on the possible designs and constraints of single-layer and multi-layer dichroic filters can be found in [6].

In this manuscript, our focus is to explore the feasibility of using a single-layer, all-metal dichroic plate with high-pass filter functionality, similar to the approach presented in [7], [8]. The primary objective of this work is to develop, validate the design, and test a prototype of such a dichroic filter. The use of an all-metal design offers the advantages of employing the dichroic filter at cryogenic temperatures, thereby minimizing system noise contributions through the improved metal conductivity and the reduced RF insertion loss, as well as reducing issues with outgassing and thermal contraction causing delamination.

For design and prototyping, we have selected the Q-band frequencies of 35-55 GHz, with a filter transmission exceeding 90% in the 37-51 GHz range and RF damping of at least 20 dB at 26 GHz. The relatively low frequency of this technology demonstrator offers the advantage of being compatible with the conventional CNC milling or similar machining techniques. Additionally, this dichroic filter can be directly utilized for the multi-band VLBI receiver system, currently under development for the Onsala Space Observatory (OSO) 20 m antenna. Nevertheless, the results of our work are also directly applicable and scalable to projects such as EHT [5], where the co-alignment of 230 GHz and 345 GHz receiver channels on the sky and dual-polarization performance are required for simultaneous observations.

In our design, we emphasize minimizing the deterioration of the frequency properties at non-normal angles of incidence (AOI) for the signal beam, as well as minimizing the cross-polarization. These considerations ensure the symmetry of the dichroic polarization response and facilitate the design of the tertiary optics. Potentially, to achieve the desired functionality at sub-THz frequencies and overcome the challenges in manufacturing small-sized all-metal components, we established microfabrication techniques, which can be employed as described in [9].

II. Background and Design Concept

For the analysis of the dichroic filter, we consider it as a single-layer metal plate with symmetrical discontinuities in the form of perforated apertures located at $n=\pm t/2$, where *t* is the thickness of the plate as depicted in Fig.1.

The plate is assumed to be illuminated by a plane wave at AOI, θ, from the direction of $z=\infty$. In the current design, the angular offset of the apertures matches the AOI, θ, as shown in Fig.1. The original problem may be decomposed into symmetric and antisymmetric wave excitations, which correspond to open and short circuit scenarios, respectively, at $z=0$. The sum of the resulting fields can then be calculated [10]. On the incident side of the plate (e.g. $n=t/2$), the electromagnetic fields are expressed as a set of Floquet modes [11].

The hollow structures inside the metal plate behave as waveguides, and the fields inside those could be considered in terms of conventional waveguide modes. The cut-off frequency values of the waveguide modes depend on the specific geometry of the apertures, such as their dimensions and shape. On the transmitted side (e.g., $n=-t/2$), the dichroic acts as an array of waveguide apertures. Each aperture, or cell re-radiates the electromagnetic waves, which are expanded again into the set of Floquet modes. The transverse aperture fields on both sides of the plate, along with the reflection and transmission coefficients could then be calculated as described in [10].

The frequency response of the dichroic filter is obtained by matching the Floquet and waveguide modes. As previously mentioned, the cut-off frequency of waveguide modes inside

the unit cells, f_{c1}, establishes the lower end of the dichroic passband. At frequencies below this cut-off, the dichroic filter behaves as a plane reflector, with the reflection coefficient increasing as the frequency decreases. In the simplified case of circular apertures with a diameter d, the passband occurs above the cut-off frequency of the dominant TE_{11} mode in the circular waveguide, which can be calculated as in [11]:

$$f_{c1} = \frac{1.841c}{\pi d}, \quad (1)$$

where c is the speed of light in free space. To optimize the frequency response of our design, we proposed a more advanced cell aperture geometry with a "snow-flake" cross-section shape and an hexagonal periodic pattern for the dichroic layout with the initial dimension a of the desired hexagonal aperture, as shown with dot lines in Fig.1. It has been demonstrated that if a regular hexagon with a side length a and a circle with diameter d have nearly the same cross-sectional area, the cut-off frequencies of the first 10 modes of waveguides with such geometry can be considered equal with an error of less than 3% [13]. Therefore, the cut-off frequency of the dominant mode in the hexagonal waveguide and the dichroic plate can be approximated as:

$$f_{c1} \approx \frac{1.841c}{a\sqrt{6\pi\sqrt{3}}}, \quad (2)$$

To achieve a cut-off frequency f_{c1} of 34 GHz, the value of a can be approximated as 2.84 mm using (2).

As mentioned earlier, the dichroic filter acts as an aperture array. The aperture pitch s (see Fig.1) determines the diffraction limit, f_{c2}. At frequencies higher than f_{c2}, when the wavelength of the incident wave is shorter than the aperture spacing values, the insertion loss of the filter increases drastically. This occurs because a portion of the power is diffracted into the first side lobe [14]. In the case of an equilateral triangular lattice with spacing s between the holes, this diffraction frequency can be expressed as

$$f_{c2} = \frac{1.1547c}{s}, \quad (3)$$

where c is the speed of light in free space. However, this diffraction into the first lobe above f_{c2} from (3) is estimated only in the case of a normal incident and zero angle of the apertures slant [7].

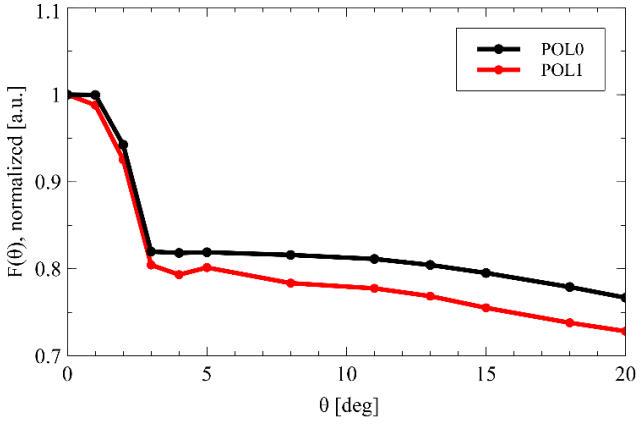

Fig. 2. The weight function $F(\theta)$, which plays a crucial role in (4) as it affects the diffraction frequency f_{c2} estimated at $\theta \neq 0$ [12], [7].

A non-normal beam incidence, $\theta \neq 0$, has a significant impact on the dichroic filters, reducing the bandwidth of the passband. This effect is known as the angular degradation. The filtering behavior of the dichroic plates with zero angle of the apertures slant at different θ values was studied in [7] by calculating the lowest Rayleigh frequency of Floquet harmonic. This frequency provides the highest limit of the filter passband and demonstrates a reduction of the passband.

However, in the current design, the slant angle of apertures is not zero and is the same as θ (see Fig.1). Therefore, the axis of the beam that comes from the z-direction will always be coaxial to the waveguide apertures in the dichroic plate. Thereby, (3) could be complemented with the empirical correction factor $F(\theta)$ introduced from our simulations, as

$$f_{c2} = \frac{1.1547c}{s} F(\theta), \quad (4)$$

Fig.2 illustrates $F(\theta)$ as a function of AOI for both horizontally E_H (POL0) and vertically E_V (POL1) oriented E–fields, respectively (as indicated in Fig.1b,e). In order to obtain $F(\theta)$, we performed HFSS 3D electromagnetic (EM) simulation of the dichroic filter as the periodic structure with the "snow-flake" shape apertures illustrated in Fig.1e. In this simulation, we estimated the diffraction limit normalized to f_{c2} (θ=0) as a function of θ (the beam axis is kept coaxial with the axis of the waveguide). More simulation results will be discussed in section III.

In practice, the undesirable effect of the angular degradation can be reduced, for instance, by changing the apertures' shape, or the use of multi-layer dichroic filters [15]. However, the multi-layer filters can have performance issues during cryogenic operation and require the implementation of cold filters and restricted apertures [15]. From (3) or (4), the diffraction limit increases with a denser perforation of the dichroic plate, which poses a challenge when designing the dichroic filter for specific purposes.

Fig.3 depicts the conceptual optical layout for the OSO multi-band receiver similar to [7]. The dichroic plate is considered to be a 3 port device that spatially separates the beams for the receiver bands. Both dichroic filters (DF1 and DF2, in Fig.3) have to be tilted to a certain angle to produce an off-axis reflection for the lower-frequency part of the RF band. However, the situation is different for the transmitted beam, as an angular degradation of the spectral properties appears to be unavoidable. As an alternative solution to multi-layer dichroic filters, in this work, we proposed a novel design concept based on tilting the waveguide inside the plate, as shown in Fig.1. It should also be mentioned that special attention is required when a specific polarization state is aimed to be maintained in the transmission or reflection. The rotation angle, α, around axis n, in the dichroic plane (see Fig.1a), is expected to produce an effect, similar to θ, resulting in a detrimental effect for the waveguide propagation modes and, consequently, reducing the passband and generating cross-polarization [15].

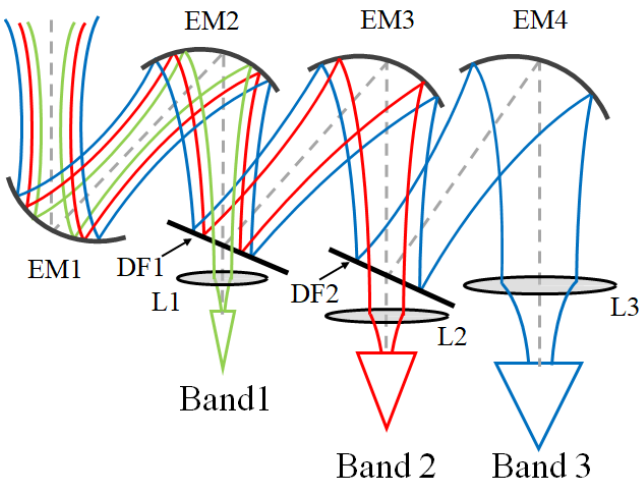

Fig. 3. The principal optical layout for the OSO multi-band receiver. The following components are marked: EM1-EM4 – ellipsoidal focusing mirrors; DF1 and DF2 – dichroic filters; L1- L3 – focusing lenses.

Furthermore, there is a trade-off between the thickness of the dichroic plate and the desired passband. The thickness of the plate determines the length responsible for the attenuation of the waves inside each waveguide perforation for the evanescent mode. A thicker plate provides a steeper cut-off slope just below the transmitted band. However, it could introduce undesired ripples in the band of interest and additional insertion loss [7].

To summarize, in order to enhance the filter passband and minimize the angular deterioration we propose a novel design of the dichroic with tilted perforations in the metal plate in combination with a customized geometry of the cell aperture.

III. Simulations Results

The frequency response of a dichroic filter is determined by geometrical parameters of the cell aperture (i.e., its shape and size), spacing between the cells, the thickness of the metal plate, and the tilt of the waveguide apertures (equals θ). Once we estimated the initial aperture dimensions and the spacing, *a* and *s,* we performed a tuning of the performance of the dichroic filter using Ansys HFSS. Fig.4a and 4b show the simulated transmission as a function of frequency at different θ values, representing POL0 and POL1 polarizations, respectively. In the simulations, the perforation's tilt angle in the metal plate follows θ. Therefore, at the incident radiation wave vector will always be coaxial to the waveguide apertures. It is observed that as θ increases, the passband where the transmission exceeds 90% becomes narrower. A value of θ=13 degrees was considered acceptable for the proposed optical layout (see Fig.3), ensuring a fractional bandwidth of over 30%.

It is worth noting that the reflected and transmitted bands for the proposed design are not separated very sharply. The frequency gap between 30 GHz and 37 GHz with transmission values of 10% and 90%, respectively, are shown in Fig.4a. This gap imposes certain operational limitations in the reflected bands. As mentioned in Section II, this cut-off slope could be made steeper using a thicker plate, nonetheless, it would introduce ripples in the response.

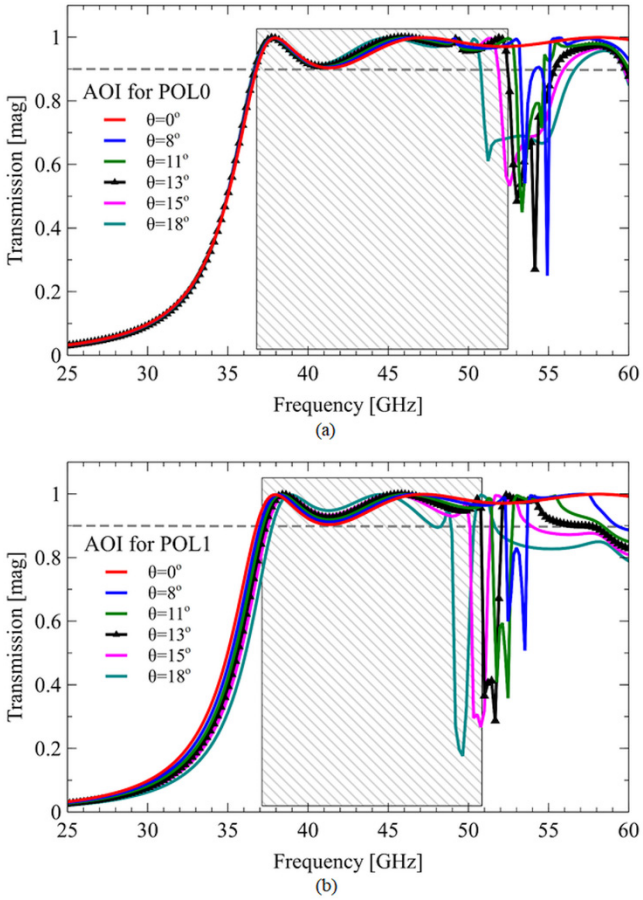

Fig. 4. The simulated transmission of the designed dichroic filter as a function of the frequency at various values of AOI: (a) for horizontally (E_H) oriented E–field (POL0); (b) for vertically (E_V) oriented E–field (POL1). The frequency ranges with transmission exceeding 90% at the design value of θ= 13 degrees, are indicated by the hatched areas. This transmission level is indicated by a grey dashed line.

When the incident beam is normal to the dichroic plate and θ=0, the simulated passband for both polarizations is maximal and reaches 65 GHz. The estimation of the diffraction cut-off frequency f_{c2} at θ=0 from (4) gives 64.5 GHz for the actual spacing distance between apertures of 5.37 mm. At other AOI values, the passband for each polarization becomes narrower due to the angular degradation.

The narrower passband observed for POL1 corresponds to different curves of $F(\theta)$, for the presented polarizations in Fig.2. This effect could likely be attributed to the collinearity of the rotating θ-axis for POL1. As illustrated in Fig.1e, the apertures are projected over the front face of the dichroic filter, orthogonal to the waveguide axis, and the plane of the incident beam is shifted in phase. That causes changes in the shape of apertures and, consequently, the length of pitch *s*. Those result in a narrower dichroic passband, e.g. slight increase of f_{c1} and a more noticeable decrease of f_{c2} (see Fig.4b). Fig.5 demonstrates the simulated cross-polarization characteristic as a function of frequency at different AOI values. From the simulations, the

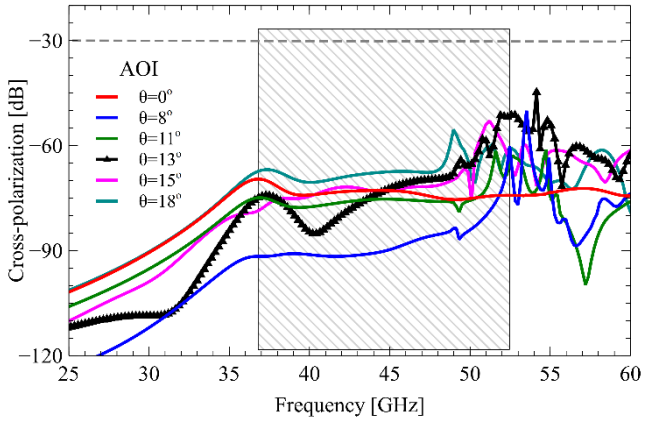

Fig. 5. The simulated cross-polarization characteristic between POL0 and POL1 of the designed dichroic filter as a function of the frequency at various values of AOI. POL0 is excited and POL1 was detected. The threshold for cross-polarization, set at -30dB, is indicated here by a grey dashed line. The hatched area indicates the frequency ranges with transmission exceeding 90% at the design value of θ=13degrees for POL0 corresponding to Fig.4a.

cross-polarization sequence shows a negligible effect on the performances. Therefore, in Fig.5 the only case represented is when POL0 was excited and POL1 was detected.

Notably, at all the presented AOI values, the leakage of the undesired polarization remains exceptionally low, consistently staying well below the threshold value of -30 dB, and denoted by a grey dashed line in the figures. This indicates that the designed dichroic filter should very effectively minimize parasitic cross-polarization.

The prototype of the dichroic filter was manufactured from a 7.11 mm thick aluminum alloy plate as shown in Fig.6. The detailed view of the "snow-flake" hexagonal cell unit is depicted in the insert of Fig.6. After the optimization process new values for a = 2.89 mm and s = 5.37 mm were found. A fillet radius, r, of the hexagon's corners, and the parameter, δ (see Fig.1b) appeared to be 0.65 mm and 0.046 mm, respectively.

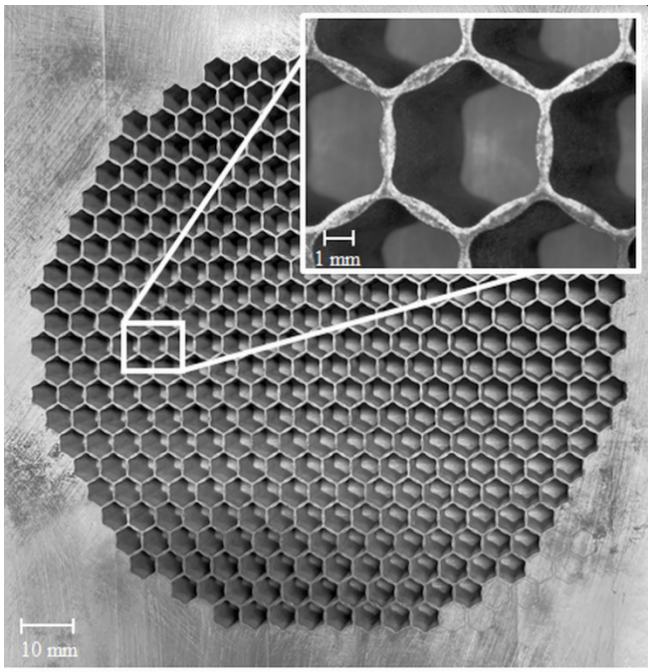

Fig. 6. Manufactured dichroic filter. The insert provides a close-up view of a single perforation cell, highlighting the details of its structure.

IV. Experimental Setup

To accurately measure the spectral performance of the fabricated dichroic filter, we designed and built a quasi-optical system that provides a plane-wave-like beam at the position where the tested dichroic is installed. The setup consists of four ellipsoidal mirrors with horn antennas at the transmitting and receiving sides. The layout of the measurement setup, visualizing the propagated beams, is illustrated in Fig.7a.

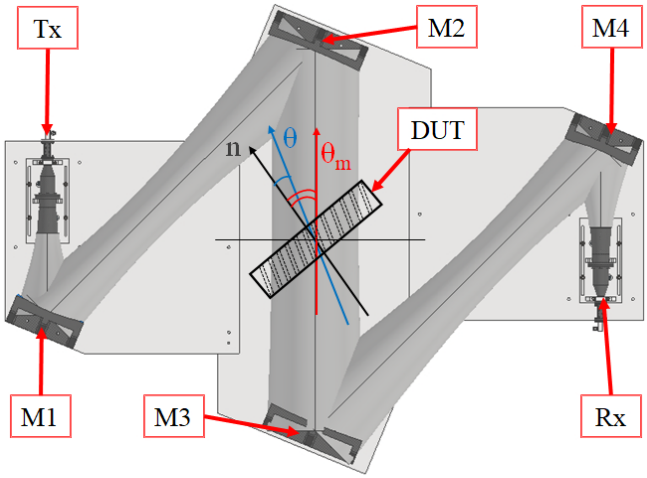

(a)

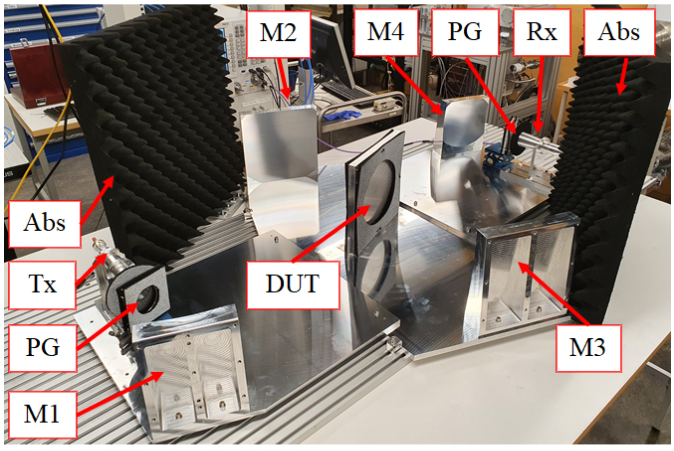

(b)

Fig. 7. The designed optical system for the characterizing the dichroic filter: (a) the schematic layout of the optical assembly, the grey-shaded volume represents the calculated quasi-optical beam indicating the path of the beam within the system; (b) a photograph of the measurement setup. The following components are marked: DUT – the dichroic filter; M1-M4 – ellipsoidal 1 focusing mirrors; PG – polarization grids; Tx and Rx – transmitting and receiving conical horns, respectively; Abs – absorber material.

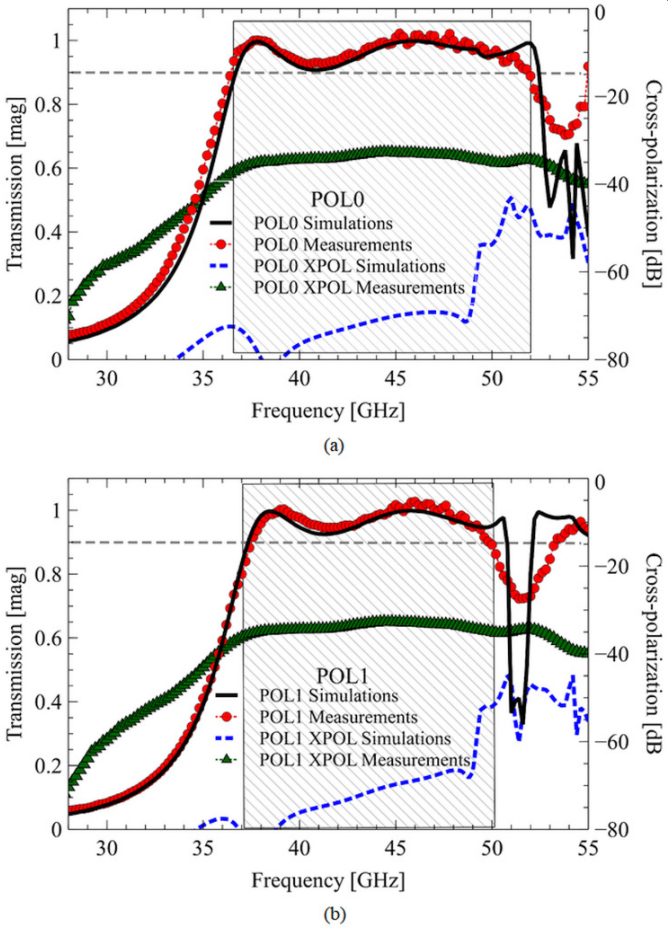

Fig. 8. Simulated and measured performance of the designed dichroic filter at nominal $\theta=\theta_m=13$ degrees: (a) for horizontally (E_H) oriented E–field (POL0); (b) for vertically (E_V) oriented E-field (POL1). The hatched area in the graph indicates the frequency range with transmission exceeding 90%, which is marked with a grey dashed line. Black solid and blue dotted lines show *simulated* values of the transmission (left Y-axis), and cross-polarization values in the logarithmic dB scale (right Y-axis), respectively. Similarly, dash lines with red circles and green up-triangles depict the *measurement* data of the transmission and cross-polarization values in the logarithmic dB scale (right Y-axis), correspondingly.

Additionally, a photograph of the measurement system is displayed in Fig.7b. The conical horn antennas with smooth spline-profile walls were optimized for the Q-band frequency range. The horns are connected to a 67 GHz Vector Network Analyzer (VNA) via a series of circular-to-rectangular and rectangular-to-coaxial adapters. One horn plays the role of the transmitter (Tx in Fig.7) while the other serves as the receiver (Rx in Fig. 7). During the measurements, the dichroic filter, referred to as a Device Under Test (DUT) in Fig.7, was positioned in the path of the collimated beam between the M2 and M3 mirrors, practically at the beam waist position, as illustrated in Fig.7b). To prevent any parasitic reflections, the area outside of 4 times the beam diameter at the dichroic plate is shielded with an absorber. Moreover, polarization grids have been incorporated into the optical system to minimize cross-polarization levels.

The incident angle θ_m represents the apparent angle between the beam axis, indicated by a red arrow in Fig.7a, and the normal direction to the metal plate n, marked with a dark grey arrow in Fig.7a.

Careful consideration was given to the design of the optical components used in the measurement setup in Gaussian optics approximation. The mirror aperture sizes were determined to be four times the width of the propagating beam ($4w_o$) ensuring that the spillover loss remained below 0.1%. Furthermore, the ellipsoidal mirrors and their positions were optimized to maintain a frequency-independent optical system. The optical train was specifically calculated for a frequency of 42.5 GHz using the methodology described in [16]. Polarization grids in front of the horns were employed to ensure the quality of cross-polarization measurements.

To calibrate out the impact of the measurement setup and ensure accurate characterization of the dichroic filter, a measurement with the presence of the dichroic and without it (but with an absorber limiting the opening, as shown in Fig.7b) was performed. The measurements were repeated for both polarizations by rotating both horns and grids by 90 degrees.

V. Measurements Results and Discussion

In order to validate the performances of the designed dichroic filter, we conducted a comparison between the simulated transmission and the measured values at θ_m=13 degrees. This angle corresponds to the nominal value of θ=13 degrees at which the perforations in the dichroic metal plate were tilted from the normal direction as illustrated in Fig.7a (marked in blue color).

The comparison was carried out for both polarization states, POL0 and POL1 as depicted in Fig.8a and b, respectively. It is evident from the figures that the measurement results closely align with the simulated transmission data exhibiting a fractional bandwidth of at least 30%. The measured low and high edges of the filter (defined as 90% transmission) passband match well with simulations with an accuracy of about 0.5 GHz. The simulated transmission at θ=13±0.5degrees demonstrates a deviation of less than 2% of the passband. This negligible deviation clearly indicates that the dichroic design is tolerant to a practical angular position accuracy of the dichroic plate, up to approximately one degree. Clearly, as an optical component, the dichroic should be placed with higher accuracy.

It is important to acknowledge that our simulations did not take into account the roughness of the metal plate surface and the perforation walls. This simplification underestimates losses and may explain the discrepancy observed in the shape of the transmission dips around 53 GHz for POL0 and 52 GHz for POL1 between the measured data and the simulations. Nevertheless, we have a very good agreement between the measurements and simulations within the dichroic RF band. The measured cross-polarization leakage remains better than 32dB across the entire passband for both polarizations, fully satisfying the practical design requirements. During the cross-polarization measurements, the dichroic apertures symmetry axis is always oriented vertically and aligned with the E-field direction of POL1 (see Fig.1). We rotated correspondingly the

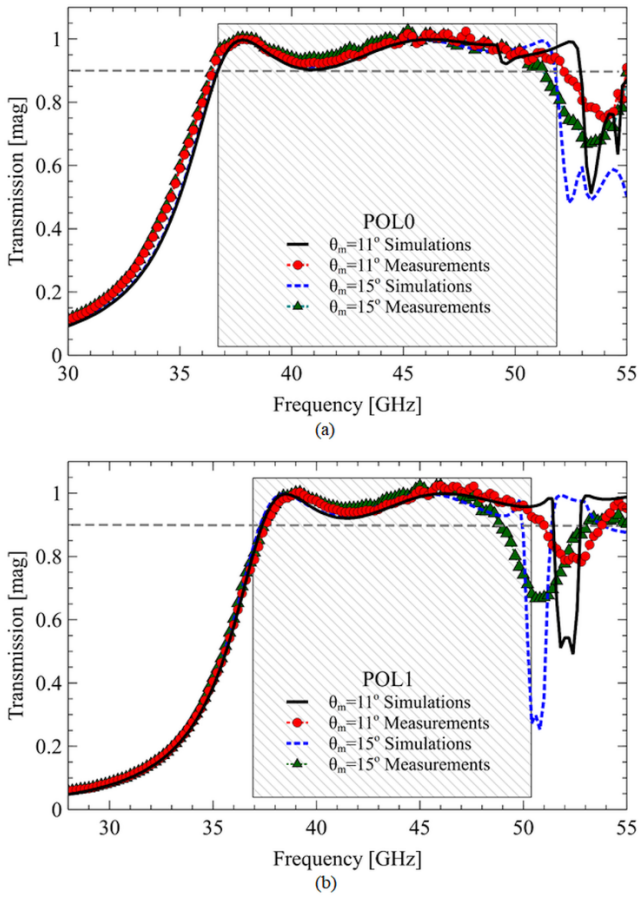

Fig. 9. Simulated and measurement results of the dichroic filter at nominal θ=13 degrees and $\Delta\theta$=±2 degrees: (a) for horizontally (E_H) oriented E–field (POL0); (b) for vertically (E_V) oriented E-field (POL1). The black solid and blue dotted lines depict the *simulation* results at θ_m=11 and 15 degrees, respectively. The dash lines accompanied by red circles (at θ_m=11 degrees) and green up-triangles (at θ_m=15 degrees) represent the *measured* transmission data of the dichroic plate. The hatched area in the graph indicates the frequency range with measured transmission exceeding 90%, which is marked with a grey dashed line at $\theta_m=\theta$ =13 degrees from Fig.8.

horn and grids at the receiver side (Rx in Fig.7). There is a noticeable difference between the measured data and simulated values of the cross-polarization. This disparity can be attributed to several reasons. The Ansys HFSS simulation model relied on perfect manufacturing and exact mathematical symmetry. Moreover, certain limitations in the experimental setup should be noted. One is specifically related to the alignment of the horns and the polarization grids over an optical path spanning, approximately two meters long. Additionally, the cross-polarization characteristic of the smooth-wall conical horns utilized in the measurements affects their accuracy.

In order to verify the accuracy of our model, we performed the measurements of the fabricated dichroic with manufactured aperture tilt of θ =13 degrees at different values of $\theta_m=\theta\pm\Delta\theta$, where $\Delta\theta$ was set to ±2 degrees and ±5 degrees (see Fig.7a). In the HFSS simulations AOI was kept always at 13 degrees and $\Delta\theta$ values were an angle between the waveguide walls axis and the incident wave axis.

The simulated transmission closely matched the measured

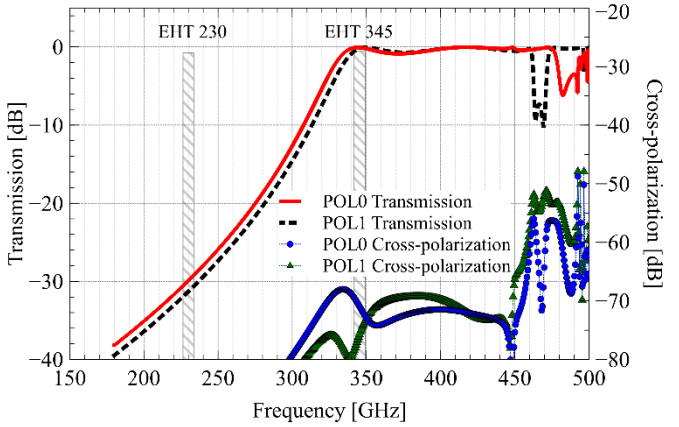

Fig. 10. Scaled simulated dichroic passband performances around 345 GHz and stop band at 230 GHz at θ=13 degrees. Solid red and dotted black lines depict transmission values for POL0 and POL1, respectively (applied to the left Y-axis). Dotted lines with blue circles and green up-triangles illustrate the cross-polarization characteristic of the dichroic filter for POL0 and POL1, respectively (applied to the right Y-axis). The hatched areas in the graph indicate 8GHz wide EHT bands of interest around 230 GHz and 345 GHz.

results for both polarizations at all four values θ_m varied in the experiments. In Fig.9 we depict a comparison between the measured transmission and the corresponding simulated values for POL0 and POL1 at $\Delta\theta$ = ±2 degrees, respectively. The measurement results proved the feasibility of the dichroic filter design with desirable frequency and polarization performance.

By scaling the dimensions with a factor of 0.11, a suitable dichroic filter could be constructed with the transmission exceeding 90% in the band around 345 GHz and lower than -30 dB at frequencies below 230 GHz. Therefore, this filter could be employed to spatially separate beams of 230 GHz and 345 GHz receiver channels for EHT with minimal contributions to the receiver noise. Fig.10 demonstrates the simulated RF performance of such a dichroic filter at the AOI of 13 degrees.

Nonetheless, given the smaller values of a and s (as small as 500 μm) along with less than 1 mm thickness of the plate and the wider bandwidth of such a dichroic filter, it will demand an advanced fabrication method combining conventional CNC machining with the all-metal micromachining method described in [9]. However, even with the fabrication accuracies provided by the micromachining method, the tolerance analysis should be addressed and the measured performances achieved in the Q-band are very challenging to preserve at higher signal frequencies.

VI. Conclusion

We have successfully designed and characterized a dichroic filter with desired RF and polarization performance. The perforation of the metallic plate has been designed and fabricated with an offset angle that corresponds to the AOI, θ=13 degrees of the incoming beam. In such a design, the tilted perforation compensates for the projected shape of the aperture when the dichroic plate is tilted, thereby minimizing the impact on the RF properties in the passband. With our design, we have

achieved a dichroic fractional bandwidth of 30% with transmission better than 90% at any frequencies within the dichroic filter passband and 96% on average. The cross-polarization level better than 32 dB over the whole passband was achieved. We demonstrated an excellent match between the simulated and measured performance. The all-metal dichroic design is fully compatible with cryogenic operation.

The presented design is also scalable to higher frequencies and could be employed as a cold dichroic filter for providing simultaneous operation at higher frequencies, for instance, the EHT 230 and 345 GHz receiver channels. For applications suitable for millimeter and THz frequencies, the filter could be fabricated using a well-established micromachining technique.

REFERENCES

[1] M. Carter, *et al.*," The EMIR multi-band mm-wave receiver for the IRAM 30-m telescope," *Astronomy & Astrophysics,* vol. 538, A89, 2012, doi: 10.1051/0004-6361/201118452.

[2] Sho Masui, *et al.*, "Development of a new wideband heterodyne receiver system for the Osaka 1.85-m mm-submm telescope - Receiver development & the first light of simultaneous observation in 230 GHz and 345 GHz bands with an SIS-mixer with 4-21GHz IF output", Publications of the Astronomical Society of Japan, vol. 73, no. 4, pp. 1100–1115, 2021, doi:10.1093/pasj/psab046.

[3] Atacama Large Millimeter/Submillimeter Array (ALMA), https://almaobservatory.org/en/home/.

[4] Seog-Tae Han et. Al., "Korean VLBI Network Receiver Optics for Simultaneous Multifrequency Observation: Evaluation," Publications of the Astronomical Society of the Pacific, vol. 125, no. 927, pp.539-547, May, 2013, doi 10.1086/671125.

[5] Event Horizon Telescope (EHT), https://eventhorizontelescope.org.

[6] Xiaolong You, Christophe Fumeaux and Withawat Withayachumnankul, "Tutorial on broadband transmissive metasurfaces for wavefront and polarization control of terahertz waves", *J. Appl. Phys*., vol. 131, no. 6, 2022, doi:10.1063/5.0077652.

[7] Letrou, C. and Gheudin, M., "Dichroic diplexer design for millimeter waves", *International Journal of Infrared and Millimeter Waves*, vol. 13, no. 1, pp. 27–42, 1992. doi:10.1007/BF01011205.

[8] D. Montofre, A. Khudchenko, F. P. Mena, R. Hesper, and A. M. Baryshev, "Single-layer dichroic filters for multifrequency receivers at thz frequencies," *IEEE Transactions on Terahertz Science and Technology*, vol. 10, no. 6, pp. 690–697, 2020, doi: 10.1109/TTHZ.2020.3025692.

[9] V. Desmaris, D. Meledin, A. Pavolotsky, R. Monje, and V. Belitsky, "All-metal micromachining for the fabrication of sub-millimetre and THz waveguide components and circuits," *J. Micromech. Microeng*., vol. 18, no.9. 2008, doi: 10.1088/0960-1317/18/9/095004.

[10] Chao-Chun Chen, "Transmission of Microwave Through Perforated Flat Plates of Finite Thickness," *IEEE Transactions on Microwave Theory and Techniques*, vol. 21, no. 1, pp. 1-6, Jan. 1973, doi: 10.1109/TMTT.1973.1127906.

[11] Robert E. Collin, "Field Theory of Guided Waves", 2nd Edition, Wiley-IEEE Press, 1991, ch.9, pp.605-643, ch.5, pp.330-348.

[12] Dong Hwi Kim, Wahab Mohyuddin, Dong Sik Woo, Hyun Chul Choi, and Kang Wook Kim, "Design of a 75–140 GHz high-pass printed circuit board", *Rev Sci Instrum.*, vol. 88, 034704, March, 2017, doi: 10.1063/1.4977935.

[13] Louis Bauer and Edward L. Reiss," Cutoff Wavenumbers and Modes of Hexagonal Waveguides," *SIAM Journal on Applied Mathematics*, vol. 35, no. 3, pp. 508-514, Nov., 1978.

[14] C. Winnerwisser, F. Lewen, and H. Helm, "Transmission characteristics of dichroic filters measured by THz time-domain spectroscopy," *Appl. Phys.A* vol. 66, pp. 593–598, 1998, doi: https://doi.org/10.1007/s003390050720.

[15] Ade, P. A. R., Pisano, G., Tucker, C., and Weaver, S., "A review of metal mesh filters", *Society of Photo-Optical Instrumentation Engineers (SPIE) Conference Series.,* vol. 6275, 2006, doi:10.1117/12.673162.

[16] Paul. F. Goldsmith, "Quasioptical Systems: Gaussian Beam Quasioptical Propogation and Applications", Wiley-IEEE Press, Jan.1998., ch2.,pp.9-38, ch.4, pp.59-68.

Daniel Montofré, received a double Ph.D. degree in electrical engineering from the Universidad de Chile, Santiago, Chile, and the University of Groningen, Groningen, The Netherlands, in 2020. After graduating he joined the Group for Advanced Receiver Development (GARD), Gothenburg, Sweden, as a postdoctoral researcher. Currently, he works as an R&D engineer at Woodtech S.A, Santiago, Chile. His research interests focus on the development of new instruments for millimeter/submillimeter space and astronomical applications, RF detection systems for Ground Penetrating Radar (GPR) applications, and quasi-optical system design.

Denis Meledin, received a Ph.D. degree in radiophysics from MSPU, Moscow, Russia, in 2003. From 2000 to 2003, he was a pre-doctoral fellow with Submillimeter Receiver Lab at Smithsonian Astrophysical Observatory, Cambridge, USA. Since 2003 he has been with Group for Advanced Receiver Development (GARD), Chalmers University of Technology, Gothenburg, Sweden. His work is related to the development of instruments for radio-telescopes (e.g., for ALMA, APEX). He focuses on designing, developing, and characterization components for radioastronomy receivers operating at microwave and mm/submm wavelengths. Besides that, he is involved in the teaching of B.S and M.S. courses and has been a co-supervisor of a number of Ph.D. students.

Cristian Daniel Lopéz was born in Buenos Aires, Argentina, in 1990. He received a B.S. degree in electronic engineering from Facultad de Ingeniería del Ejército Grl. Div. Manuel N. Savio, Buenos Aires, Argentina, in 2012, and the M.Sc. degree in microelectronics from Universidad Politecnica de Cataluña, Barcelona, Spain, in 2018.

Mr.Lopéz is currently working toward a Ph.D. degree at Chalmers University of Technology, Gothenburg, Sweden. His current research interests are the design and characterization of cryogenic components for THz systems.

Igor Lapkin received his M.Sc. degree from the Technical State University, Nizhny Novgorod, Russia, in 1985. He currently holds the position of Senior Researcher Engineer at the Group for Advanced Receiver Development, GARD, Department of Space, Earth, and Environmental Sciences, Chalmers University of Technology, Gothenburg, Sweden. His current interests are designing and developing components, mixers, and heterodyne receivers for radio astronomy.

Vincent Desmaris received the M.Sc. degree in material science from the National Institute of Applied Science, Lyon, France, in 1999, and the Ph.D. degree in electrical engineering from the Chalmers University of Technology, Gothenburg, Sweden, in 2006. His thesis concerned the fabrication, characterization, and modeling of AlGaN/GaN microwave transistors.

Since 2006, he has been with the Group for Advanced Receiver Development (GARD), Chalmers University of Technology and currently serves as a Head of GARD. His research interests include the area of terahertz receiver technology, especially microfabrication and characterization of waveguide components and circuits and planar cryogenic microwave devices.

Leif Helldner, Leif Helldner was born in Onsala, Sweden in 1969. Since 1988, he has been a Research Engineer at Onsala Space Observatory.
His main expertise are mechanical design of cryogenic receiver systems for radio astronomy.
He has been involved in developing receiver systems for radio telescopes and projects as ALMA, APEX, SEST, SKA, VLBI 2010.

Mathias Fredrixon received the B.S. degree in engineering from the Chalmers University of Technology, Gothenburg, Sweden. Since 1998, he has been working at the Group for Advanced Receiver Development, GARD, Onsala Space Observatory, Chalmers University of Technology, Gothenburg, Sweden.

He is currently working as senior research engineer and the main field is mechanical design and development of measuring systems and receivers for radio astronomy. He actively participated in developing ALMA Band 5 and Band 2 receivers, in development and support instruments for the APEX telescope in Chile, in the Swedish Odin satellite and Hershel space telescope projects.

Sven_Erik Ferm, photograph and biography is not available at the time of publication.

Victor Belitsky (Senior Member, IEEE) (M'95–SM'07) received the M.Sc. degree in electrical engineering from the Moscow Telecommunication Institute in 1977, and the Ph.D. degree in experimental physics from the Institute of Radio Engineering and Electronics, U.S.S.R. Academy of Sciences, Moscow, Russia, in 1990.

He is currently Professor at the Group for Advanced Receiver Development, Department of Space, Earth, and Environmental Sciences, Chalmers University of Technology, Gothenburg, Sweden.

Research interests of Prof. Belitsky include terahertz and superconducting electronics and components, instrumentation for radio astronomy, and environmental science.